Available online at www.sciencedirect.com
SCIENCE DIRECT®
Journal of Constructional Steel Research 61 (2005) 1–21
JOURNAL OF CONSTRUCTIONAL STEEL RESEARCH
www.elsevier.com/locate/jcsr

Cyclic behaviour of unreinforced and rib-reinforced moment connections

Cheng-Chih Chen*, Shuan-Wei Chen, Ming-Dar Chung, Ming-Chih Lin

Department of Civil Engineering, National Chiao Tung University, 1001 Ta Hsueh Road, Hsinchu 30010, Taiwan

Received 9 February 2004; accepted 29 June 2004

Abstract

This study investigates the cyclic behaviour of the beam-to-column welded moment connections used in steel moment-resisting frames. Two unreinforced welded connections were tested initially to elucidate the behaviour and failure mode. Test results showed that both specimens failed by the brittle fracture of the beam flange, initiated from the root of the weld access hole. Nonlinear finite element analysis was used to identify the causes of the failure. The stress concentration in the weld access hole region has the potential to cause the beam flange to fracture. Analytical results also demonstrated that reinforcing the connection with a single rib can reduce the concentration of stresses at the root of the weld access hole. Further tests of two specimens whose beam flanges were each reinforced by a single rib revealed that the single rib effectively prevents beam flange fracture in the weld access hole region.

Keywords: Welded moment connection; Weld access hole; Flange rib; Plastic rotation

* Corresponding address: Department of Civil Engineering, National Chiao Tung University, 1001 Ta Hsueh Road, Hsinchu 30010, Taiwan. Tel.: +886 3 571 2121x54915; fax: +886 3 572 7109.
E-mail address: chrischen@mail.nctu.edu.tw (C.-C. Chen).

0143-974X/$ - see front matter © 2004 Elsevier Ltd. All rights reserved.
doi:10.1016/j.jcsr.2004.06.005

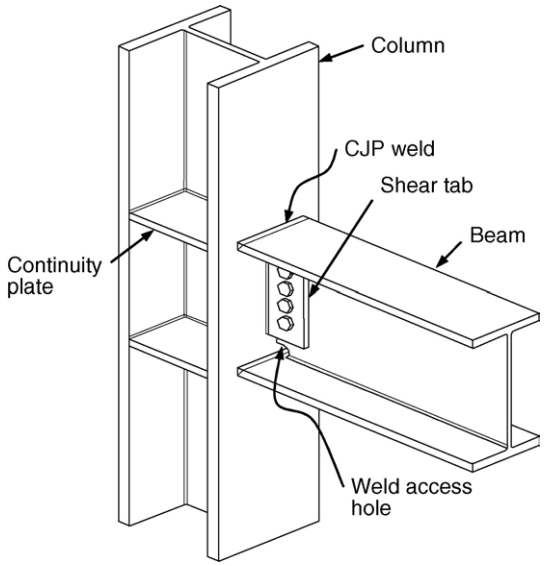

Fig. 1. Typical pre-Northridge beam-to-column moment connection.

1. Introduction

Steel moment-resisting frames are believed to be able to develop the strength and ductility required to resist strong seismic loading because steel is ductile. The 1994 Northridge earthquake caused widespread damage to moment-resisting frames [1–3]. Various brittle fractures were found in beam-to-column welded moment connections. Typical pre-Northridge welded moment connections were designed to transfer the flexural moment and shear force of beams to columns. Fig. 1 depicts the configuration of a typical moment connection used in moment-resisting frames. A bolted shear tab is commonly used to transfer the shear force, and a complete joint penetration (CJP) groove weld is employed in the field to join the beam flange to the column flange. The beam-to-column interface is the critical section that has the maximum flexural moment when moment frames are subjected to earthquake-induced forces. Therefore, fractures usually initiate at the CJP weld between the beam flange and column flange. The brittle failure prevents the welded moment connections from exhibiting the inelastic behaviour expected to resist earthquake loading.

Numerous studies have been undertaken to improve the behaviour of the pre-Northridge moment connection. The improvement is based mainly on strengthening the connection [4–7] or weakening the beam [8–10] to develop stable inelastic behaviour that will dissipate a large portion of the energy absorbed from the earthquake. The inelastic behaviour of the connection is attributed mainly to the formation of a plastic hinge in the beam, so improvement attempts aim to ensure the formation of a plastic hinge at the desired location in the beam. This work aims to elucidate and improve the performance of the welded moment connection. Two unreinforced moment connections were tested initially to

clarify the cyclic behaviour and the failure mode. An analytical study was performed using nonlinear finite element analysis to improve understanding of the performance of such connections and predict the brittle behaviour. On the basis of experimental and analytical findings, two rib-reinforced connections were further tested to examine their performance.

2. Unreinforced connection tests

2.1. Specimens

Two large-scale specimens were fabricated and tested to clarify the behaviour and failure mode of the pre-Northridge connection. These two specimens represent an exterior beam-to-column connection. Fig. 2 presents the details concerning the connection of the specimens. The specimens comprised an A36 beam and an A572 Gr. 50 column. The weld access hole had to be cut on the beam web to enable the full penetration groove welding between the beam flange and the column flange. A quarter-circular shape weld access hole used by the steel manufacturers was adopted herein. Fig. 3 illustrates the geometry of the weld access hole, which indicates a small radius, allowing a smooth join between the web and the flange. Meanwhile, as recommended by FEMA [11], the backup bar used in the full penetration weld in the beam bottom flange was removed using a carbon arc and a fillet weld was added. However, the backup bar on the top flange of the beam remained in place but a fillet weld was added to weld the backup bar to the beam flange and the column flange, as indicated in Fig. 2.

2.2. Test set-up and procedure

Fig. 4 illustrates the test set-up for the specimens. Hinged supports were provided at both ends of the column, and lateral braces were used to prevent lateral deformation of the beam. A predetermined cyclic displacement history, following the ATC testing protocol [12], was applied to the beam tip. Fig. 5 plots the cyclic deformation history. Displacement amplitudes were specified in multiples of Δ_y, which represents the displacement at the cantilever end when the beam reached its yield moment capacity. The specimens were subjected to three cycles with displacement amplitudes of 0.25, 0.5, 0.75, 1.0, 2.0 and $3.0\Delta_y$, and two cycles with amplitudes of over $3.0\Delta_y$ until failure occurred. The yielding displacement Δ_y was 15 mm for specimen S6, representing a storey drift angle of 0.45% rad, while that for specimen S7 was 20 mm, representing a 0.60% rad storey drift.

2.3. Test results

The beam flanges close to the column in both specimens developed moderate inelastic behaviour. The yielding pattern of the beam flange of specimen S6 can be observed in Fig. 6. No sign of local buckling of the beam was observed before failure. Fig. 7 plots the maximum moment in the beam versus the total plastic rotation for both specimens. The moment was computed at the column face based on the load obtained from the actuator. The moment, M, was also normalized by the plastic flexural strength of the beam, M_p, according to material strengths measured in the tensile coupon test. The total plastic

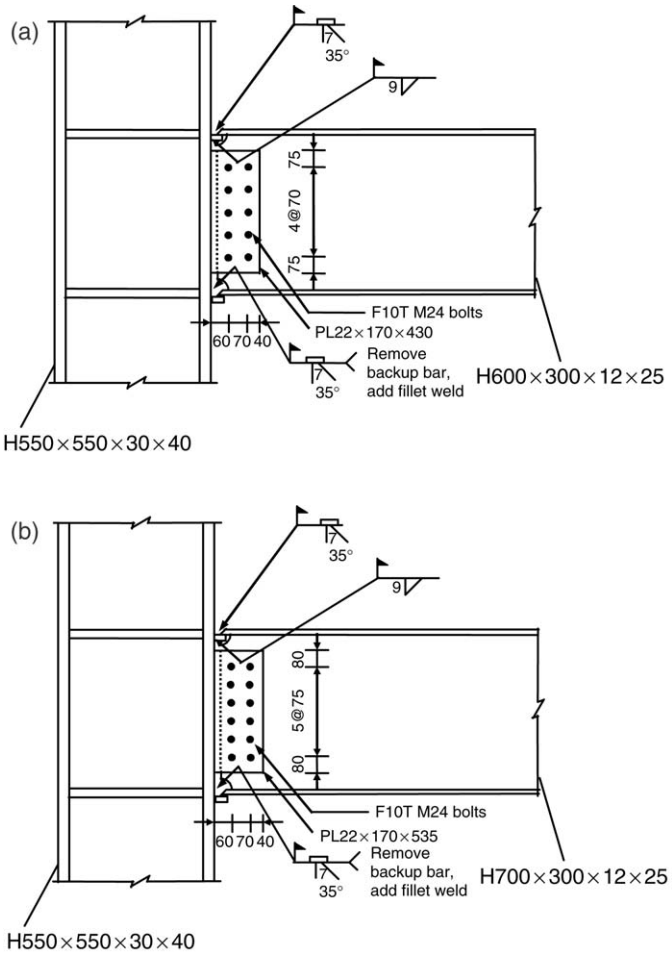

Fig. 2. Connection details for two unreinforced connection specimens: (a) specimen S6; (b) specimen S7.

rotation, θ_p, was obtained by subtracting the elastic rotation from the total rotation of the specimens, θ_{total}, which was determined by dividing the displacement of the beam tip by the distance from the beam tip to the centre of the column. Hence

$$\theta_p = \theta_{\text{total}} - \frac{M}{K_\theta} \tag{1}$$

where K_θ is the elastic rotational stiffness of the specimen. Neither hysteresis curve in the figure reveals degrading of strength. Specimen S6 exhibited a total plastic rotation of only 1.9% rad corresponding to a maximum storey drift of 3.15% rad, while specimen S7 exhibited a total plastic rotation of 2.4% rad corresponding to a maximum storey drift of 3.6% rad. However, both specimens developed flexural moments greater than the plastic flexural strengths of the beam section.

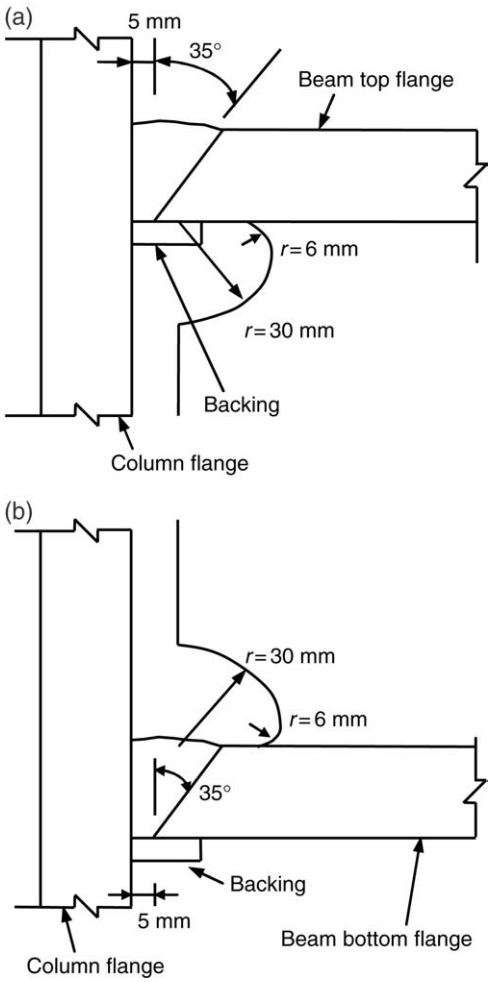

Fig. 3. Details of the weld access hole and groove weld: (a) top flange; (b) bottom flange.

2.4. Failure mode

Both specimens failed catastrophically. The failures were caused by the fracture of the beam flange initiated at the intersection between the weld access hole and the full penetration weld. The fractures propagated toward the flange edges and caused the beam flange to fail. The two specimens exhibited identical failure modes, as illustrated in Figs. 6 and 8. The photographs shown in Fig. 8 represent a close look at the fracture of the beam flange of specimen S7 at the end of the test. Similar fractures were observed in the tests conducted by Stojadinovic et al. [13] and Azuma et al. [14]. The fracture may have been initiated at the weld access hole because of localized stress concentration, which assertion will be addressed in the following section using nonlinear finite element analysis.

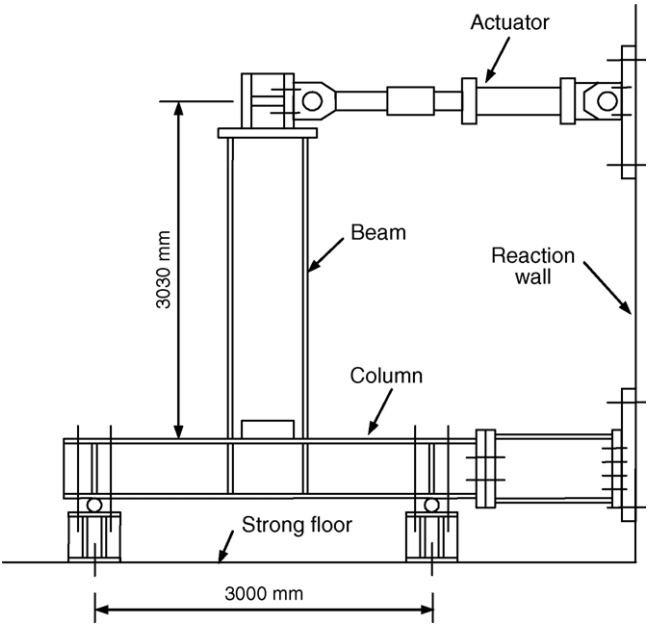

Fig. 4. Schematics of the test set-up.

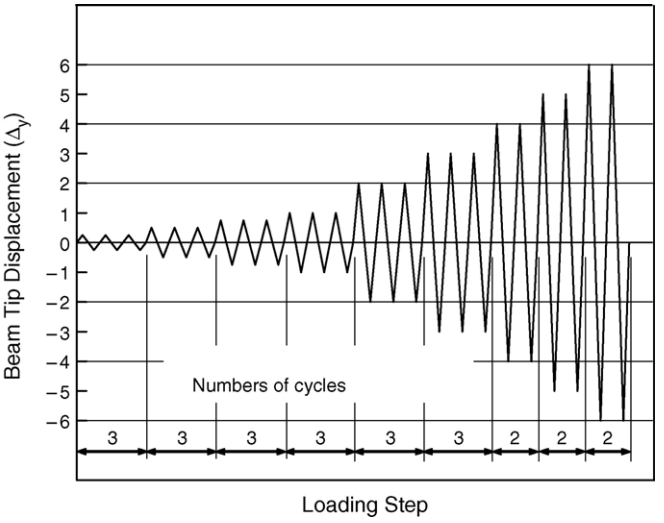

Fig. 5. The test protocol.

3. Finite element analysis

Nonlinear finite element analysis was performed to examine the stress and strain distributions at the connection. Specimen S6 was modelled using the finite element program. Results of the simulation of the tests were compared with the actual test results

Fig. 6. Yielding and fracture of the beam flange of specimen S6.

to confirm the finite element model. The established finite element model was further employed to investigate the reinforcing scheme used to improve the behaviour of the pre-Northridge connection.

3.1. Modelling

The general purpose finite element program ANSYS [15] was used in the analytical studies. A finite element model was generated accurately to represent the specimen. Elements were properly generated to capture fully the behaviour of the connection. Fig. 9 depicts the mesh of the finite element model of specimen S6. The symmetry in the plane of the beam and the column webs was such that only half of the specimen was modelled and analysed to reduce computational effort. An eight-node, three-dimensional solid element with 24 nodal degrees of freedom was used to model the structural steel. The model of specimen S6 consisted of 14,669 nodes and 8,900 elements. Constraints that were consistent with the test set-up were applied in the model. A displacement control analysis incremented displacement of the beam tip, which was identical to the testing protocol.

Stress–strain relationships were obtained from a coupon test to model the material properties of the steel. Steel usually exhibited linear elasticity, followed by a yield plateau, and then strain hardening up to the ultimate strength. Accordingly, the yield strength measured in material coupon tests was used as an analytical property of the material. However, the measured stress–strain relations were simplified as a bilinear relationship with strain hardening, with a 4% modulus of elasticity. Furthermore, the behaviour of steel under compression was assumed to be the same as that under tension. The von Mises yield criteria were used to specify the plasticization.

3.2. Analytical results for specimen S6

The predictions of the finite element analysis were compared with the experimental results in terms of load and deformation relations to verify the analytical model. Fig. 10

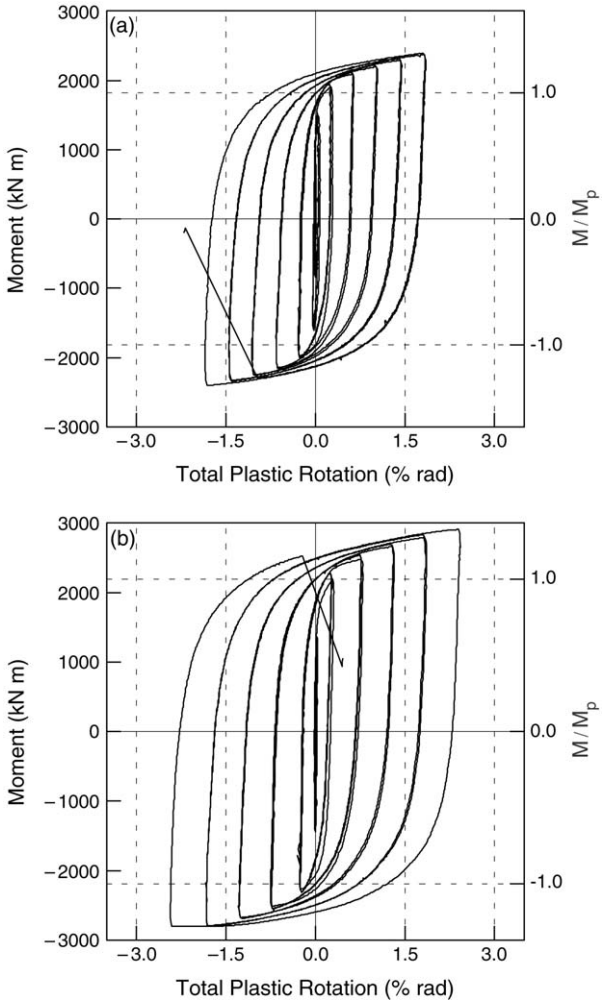

Fig. 7. Hysteresis curves of unreinforced connection specimens: (a) specimen S6; (b) specimen S7.

plots the beam tip load versus the displacement for specimen S6, as determined by finite element analysis and experimentally. The results are consistent with each other. The analytical results are also plotted in the form of a stress distribution to elucidate the yielding and plasticization of the connection. Fig. 11 displays the von Mises stress distribution in the beam-to-column joint and the adjacent beam section at a plastic rotation of 3% rad because SAC [16] recommended a 3% rad minimum plastic rotation capacity for the connection of the moment frames. The beam flange yielded near the column face because the critical section through which the beam forces were transferred to the joint was the joint–beam interface. Localized stress concentrations were observed in the beam-to-column interface and in the weld access hole region, owing to the geometric discontinuity at the joint.

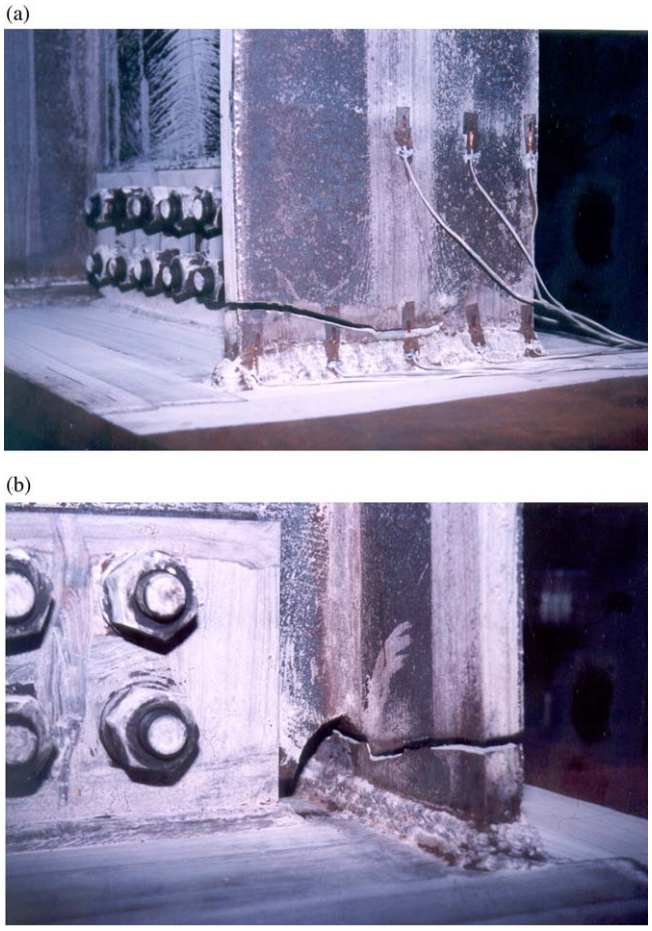

Fig. 8. Specimen S7 after failure.

Additionally, the highest stress was in the vicinity of the weld access hole, from which the beam flange fractured during the test.

3.3. Modelling of rib-reinforced connections

Connections strengthened by vertical rib plates were analysed to find ways to reduce the stress concentration localized near the weld access hole. Welding the vertical rib plates to the beam and column flanges is intended to reduce the connection's stress demand on the complete penetration weld in the beam flange and move the plastic hinge away from the face of the column. Two finite element models were constructed to study the effect of the rib on the behaviour of the connection. Fig. 12(a) presents the connection strengthened with two separate rib plates on the top and bottom beam flanges. Notably, only half of the connection was modelled because the connection is symmetrical in the plane of the beam and column webs. The model used a beam and a column of the same size as those for

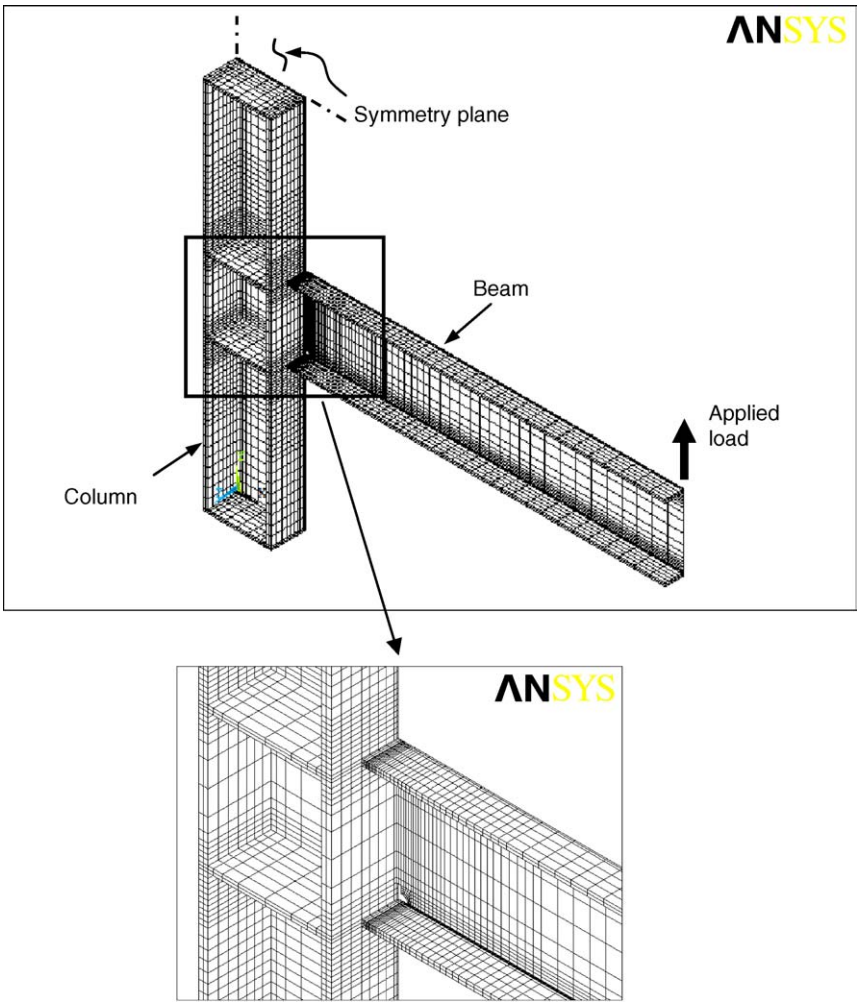

Fig. 9. The three-dimensional finite element mesh for specimen S6.

specimen S6. The triangular rib plate was 20 mm thick, 100 mm high and 200 mm long. Engelhardt et al. [17] tested this type of connection. Their test results indicated that two specimens exhibited a plastic rotation of 2.5 and 3% rad, and failed by the gradual tearing of the beam flange at the tips of the rib plate.

The other finite element model used only a single rib welded to the centreline of the beam flange, as illustrated in Fig. 12(b). The single rib is located in the same plane as the column web to enhance the transfer of the force from the beam to the column. However, there is very little information on the behaviour of connections reinforced with a single rib. This single-rib (SR) connection used a rib plate of the same size as that used for the double-ribs (DR) connection.

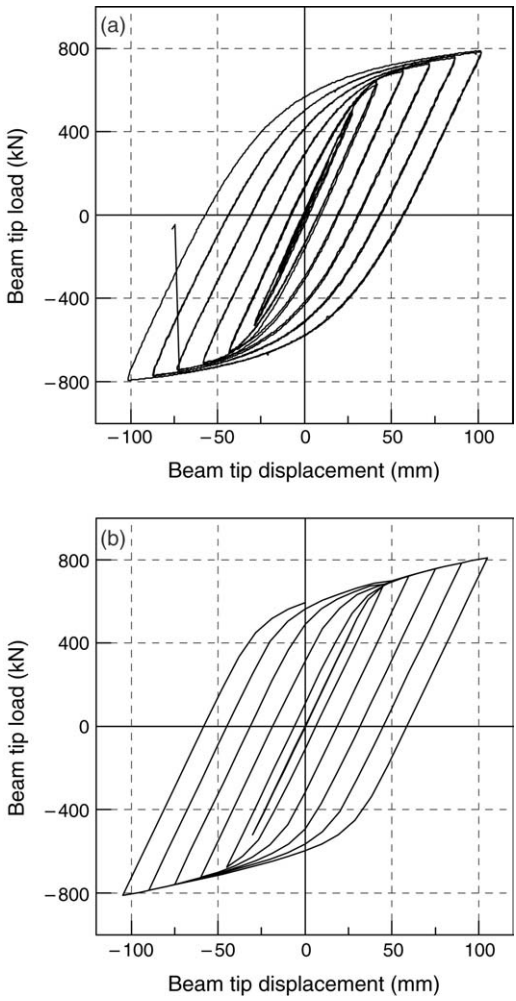

Fig. 10. Experimental and analytical hysteresis curves for specimen S6: (a) experiment; (b) finite element analysis.

3.4. Analytical results for rib-reinforced connections

Analytical results are examined for the stress distribution and the spread of the yielding zone in the joint. Fig. 13 plots the von Mises stress distributions in the joint for DR and SR connections at a plastic rotation of 3% rad. Both connections revealed that extensive yielding of the beam section occurred away from the column face, such that the plastic hinge in the beam for both specimens was developed at the same place in spite of the different reinforcement of the ribs. Nevertheless, the von Mises stress in the DR connection was maximum in the access hole region, while that in the SR connection was maximum in the beam flange at the rib tip.

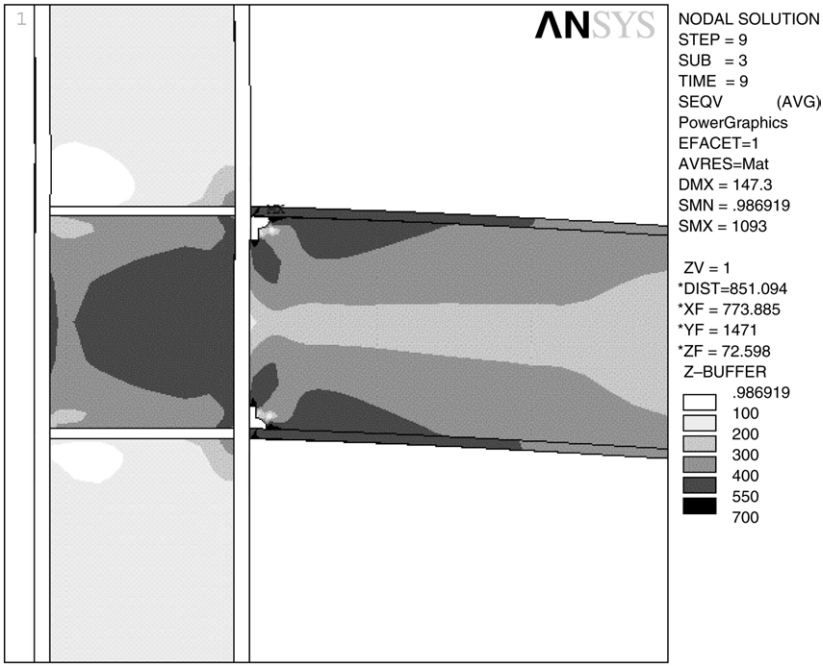

Fig. 11. The von Mises stress distribution for specimen S6.

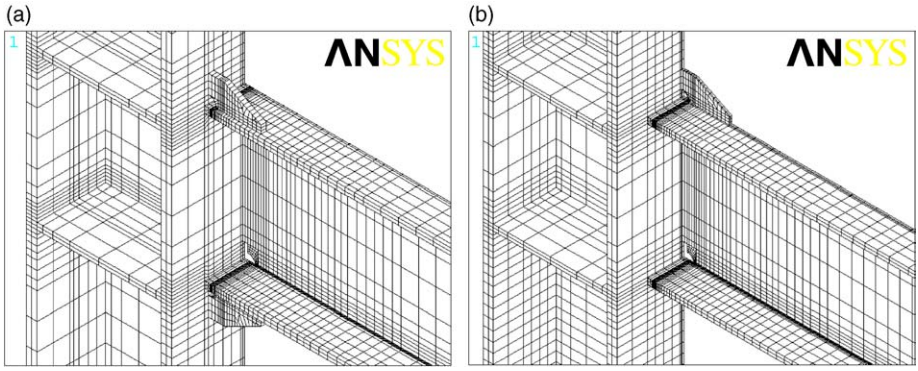

Fig. 12. Meshes in the joint for rib-reinforced connections: (a) double-ribs (DR) connection; (b) single-rib (SR) connection.

Fig. 14 presents the beam tip load versus total rotation for specimen S6, DR and SR connections, to examine the global behaviour of the connections. The curves for DR and SR connections were virtually identical because both connections formed plastic hinges in the beam beyond the rib tip. Both DR and SR connections exhibited a higher ultimate capacity than specimen S6, but had the same elastic stiffness, because both connections were shorter from the beam tip to the plastic hinge than in specimen S6.

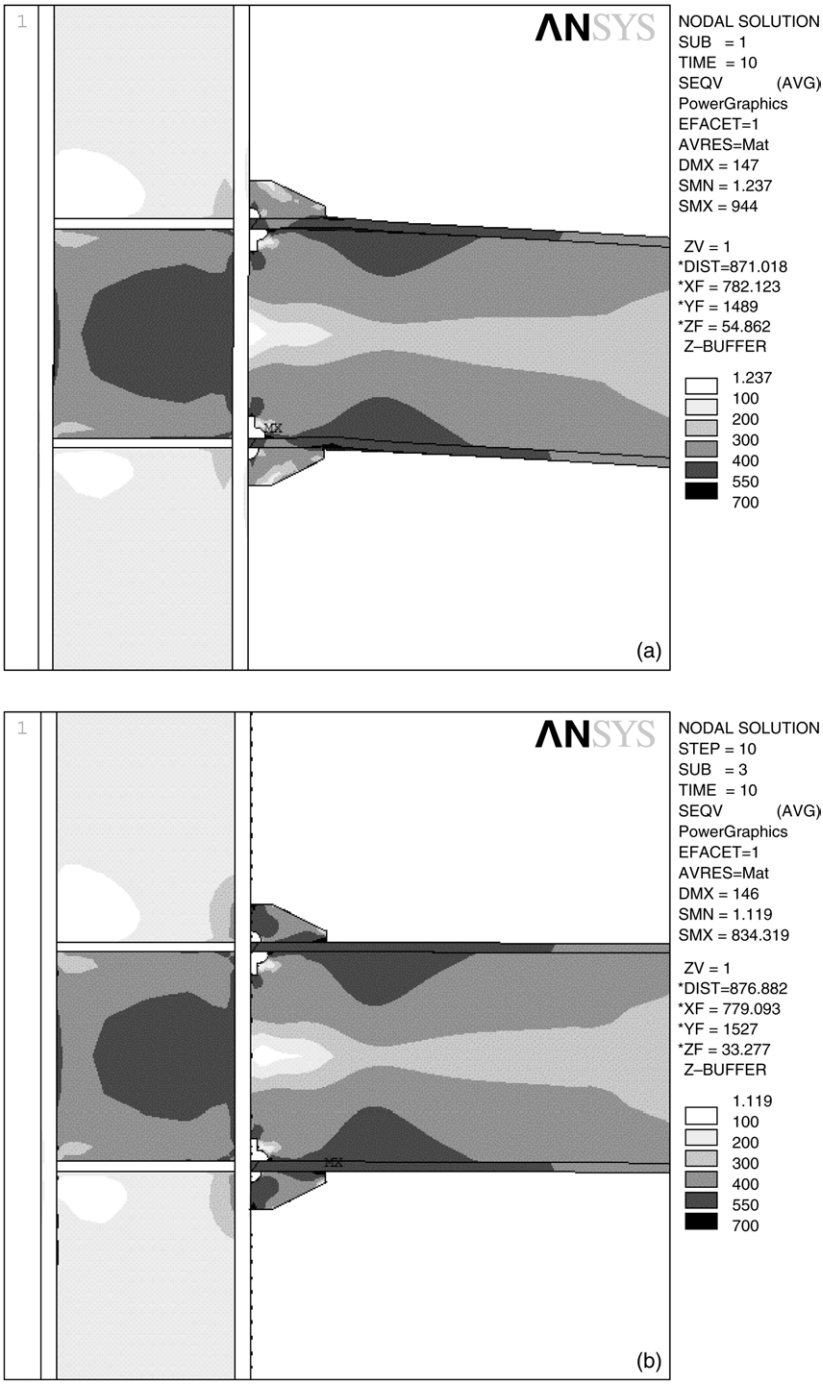

Fig. 13. The von Mises stress distribution for rib-reinforced connections: (a) DR connection; (b) SR connection.

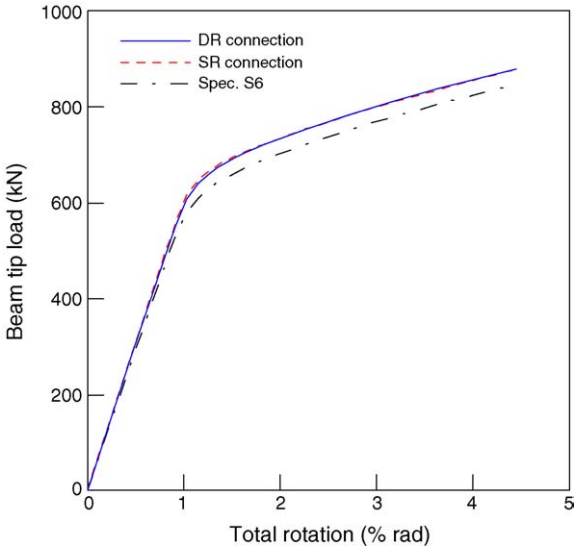

Fig. 14. Load versus total rotation relations for various connections.

The distributions of stress and strain along the width of the beam flange were studied in two critical sections to clarify the stress distribution and strain demand in the beam-to-column joint. Line CJP in Fig. 15 represents the position at which the complete joint penetration groove weld joins the beam flange and column flange. Line WAH is at the root of the weld access hole, where fracture occurred during the test. The pre-Northridge connections failed at limiting plastic rotation, so the stress and strain distributions when minor inelastic behaviour occurs are of interest. A 0.25% rad plastic rotation was considered to represent this stage. The analytical results concerning the other stage, represented by 3% rad plastic rotation, were studied to examine the highly strained behaviour of the joints.

The results of finite element analyses are presented in the forms of the normalized longitudinal stress and PEEQ index. The longitudinal stress, σ_{11}, represents the normal stress in the beam flange and is normalized by the yield stress F_y of the beam material. The PEEQ index is defined as the plastic equivalent strain (PEEQ) divided by the yield strain ε_y of the beam material, which represents local strain demand [18]. The plastic equivalent strain is defined as

$$\text{PEEQ} = \sqrt{\frac{2}{3}\varepsilon_{ij}\,\varepsilon_{ij}} \tag{2}$$

where ε_{ij} is the component of plastic strain in the direction specified by i and j. In the ANSYS finite element program, the PEEQ is denoted as the EPEQ, which is the equivalent plastic strain.

Fig. 16 plots the resulting normalized longitudinal stresses and PEEQ indices along Lines CJP and WAH at 0.25% rad plastic rotation. Both DR and SR connections effectively reduced the longitudinal stresses at the CJP weld and WAH below those of the unreinforced

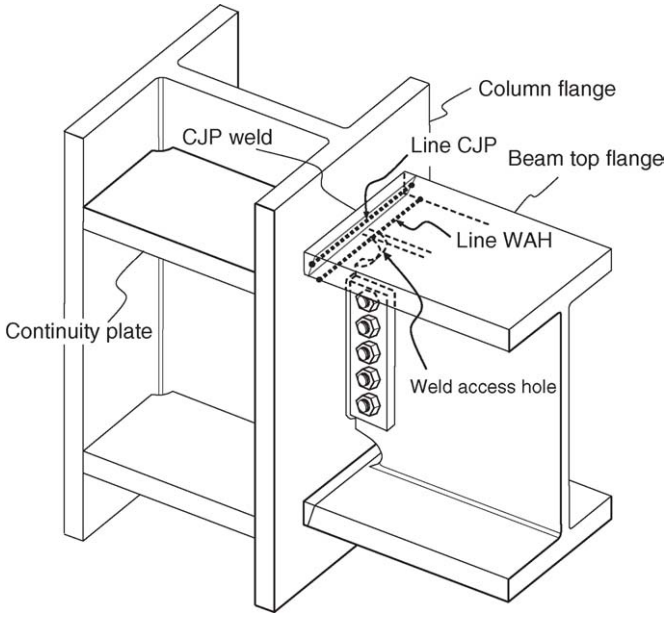

Fig. 15. Lines in the critical section.

specimen S6, although DR and SR connections demonstrated similar longitudinal stress distributions. Strain was concentrated at the root of the access hole, as plotted in Fig. 16(d). Nevertheless, the SR connection was more effective than the DR connection in reducing the concentration of strain, especially at the root of the access hole, as indicated in Fig. 16(d).

Fig. 17 plots normalized longitudinal stresses and PEEQ indices at a plastic rotation of 3% rad. The presence of the rib significantly decreased the stress and strain demand along Lines CJP and WAH. The maximum values of the PEEQ indices at the root of the access hole shown in Fig. 17(d) were 23.1, 13.8 and 9.6 for specimen S6, the DR connection and the SR connection, respectively. The SR connection very significantly reduced the PEEQ index at the root of the access hole, implying that the single rib could reduce the potential for the beam flange to fracture near the access hole region.

4. Rib-reinforced connection tests

4.1. Specimens

On the basis of the finite element analysis, two specimens were designed with reinforced connections. A single rib was welded to the centreline of each beam flange. Fig. 18 presents the details of the connection. The height of the rib was designed to be less than the thickness of the concrete slab. Both specimens had triangular ribs 100 mm high and 200 mm long, but with different thicknesses. The rib plate of specimen SR30 was 30 mm thick, while that of specimen SR20 was 20 mm thick. The ratios of plastic flexural strength of the rib

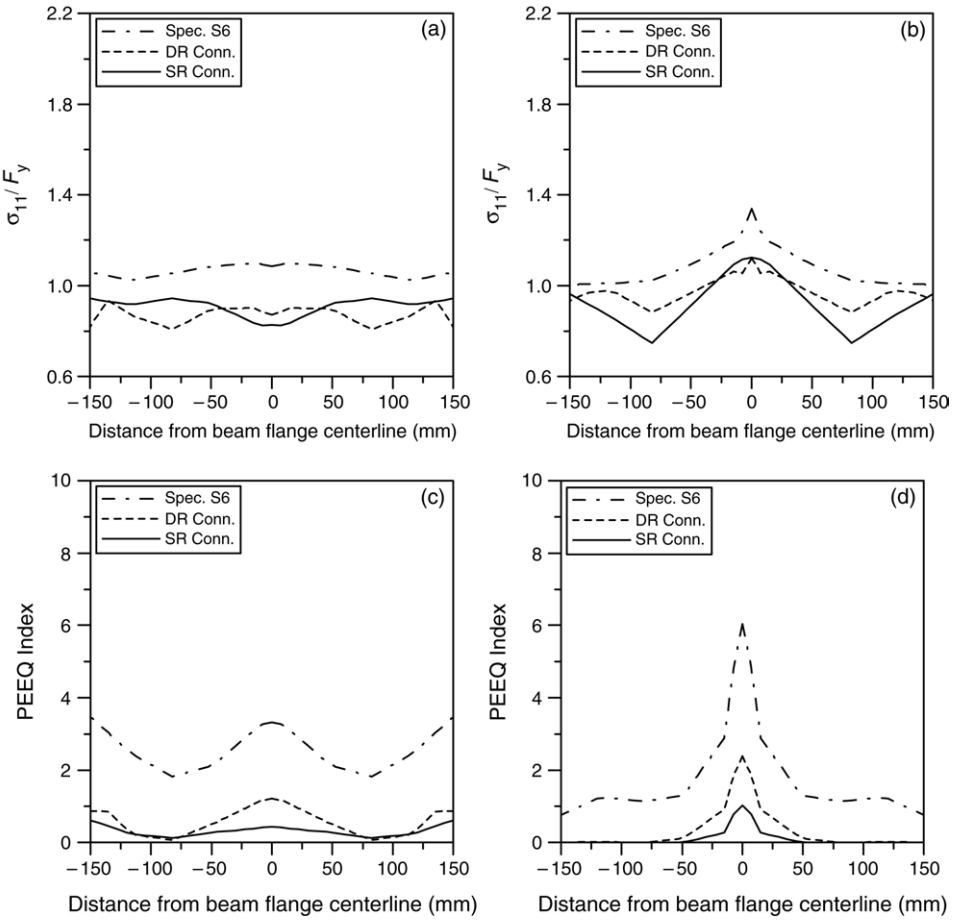

Fig. 16. Longitudinal stresses and PEEQ indices at 0.25% rad plastic rotation: (a) longitudinal stresses along Line CJP; (b) longitudinal stresses along Line WAH; (c) PEEQ indices along Line CJP; (d) PEEQ indices along Line WAH.

to that of the beam section, $Z_{\text{rib}}F_{\text{rib}}/ZF_y$, at the beam-to-column interface were 0.36 and 0.24 for specimens SR30 and SR20, respectively. Z_{rib} and Z represent the plastic moduli for the cross sections of the rib plate with maximum height and the beam, respectively, and F_{rib} and F_y are the measured yield strengths of the rib plate and the beam, respectively. Specimens consisted of the same rolled shape beam H588 × 300 × 12 × 20, confirmed to be of ASTM A36 materials with a yield strength of 304 MPa.

4.2. Test results and discussion

4.2.1. Behaviour and failure mode

The test set-up and procedure were identical to those of the tests of unreinforced connections. Specimen SR30 yielded in the beam flanges beyond the rib tip during the

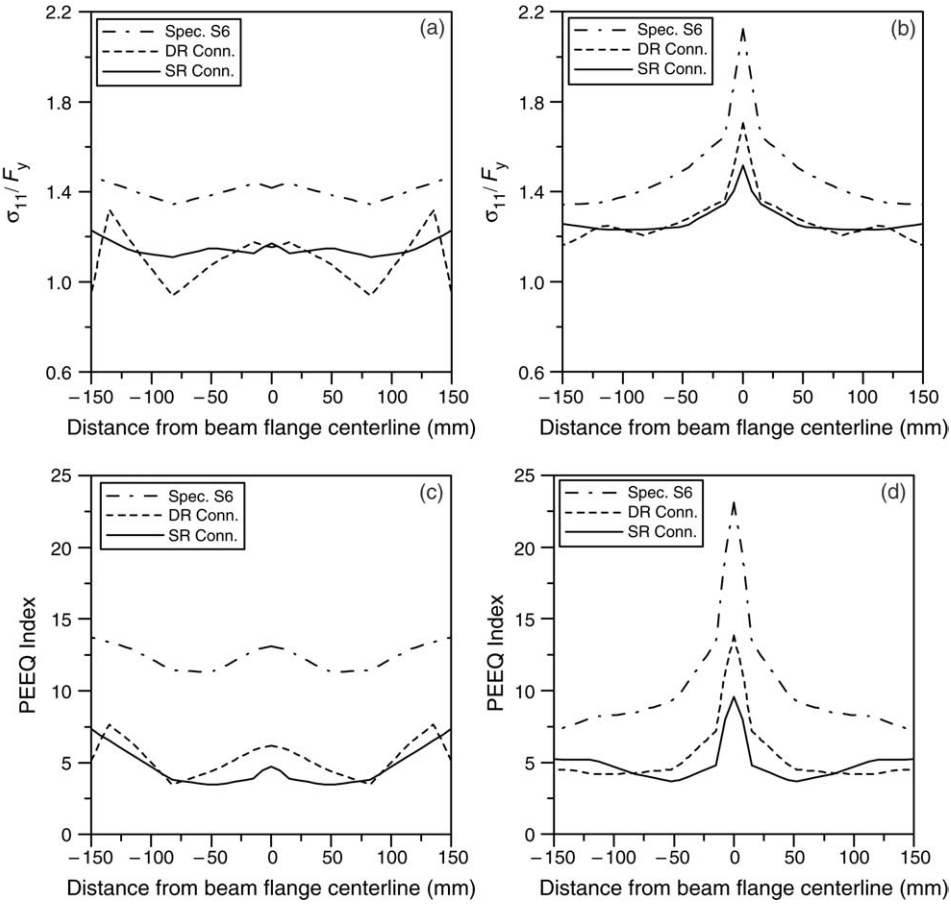

Fig. 17. Longitudinal stresses and PEEQ indices at 3% rad plastic rotation: (a) longitudinal stresses along Line CJP; (b) longitudinal stresses along Line WAH; (c) PEEQ indices along Line CJP; (d) PEEQ indices along Line WAH.

cycles of 1% rad storey drift. The beam flanges underwent slight local buckling at a storey drift of 2.3% rad. A minor crack in the bottom flange of the beam at the rib tip was detected at a storey drift of 2.8% rad. This crack grew slowly but propagated toward the base metal of the beam flange. This ductile tearing of the base metal gradually reduced the strength of the connection. Fig. 19 shows the fracture of the beam flange at a storey drift of 4.1% rad; the test was terminated during these cycles because of a great loss of strength.

Before the cycles associated with 2.3% rad storey drift, the behaviour of specimen SR20 was quite similar to that of specimen SR30. The top flange of the beam cracked at the rib tip at a storey drift of 2.3% rad. Unlike the crack in specimen SR30, this crack did not grow. In contrast, specimen SR20 failed with a very loud bang caused by the fracture of the beam top flange at a storey drift of 2.8% rad. This brittle crack led to complete fracturing of the top flange of the beam, as displayed in Fig. 20.

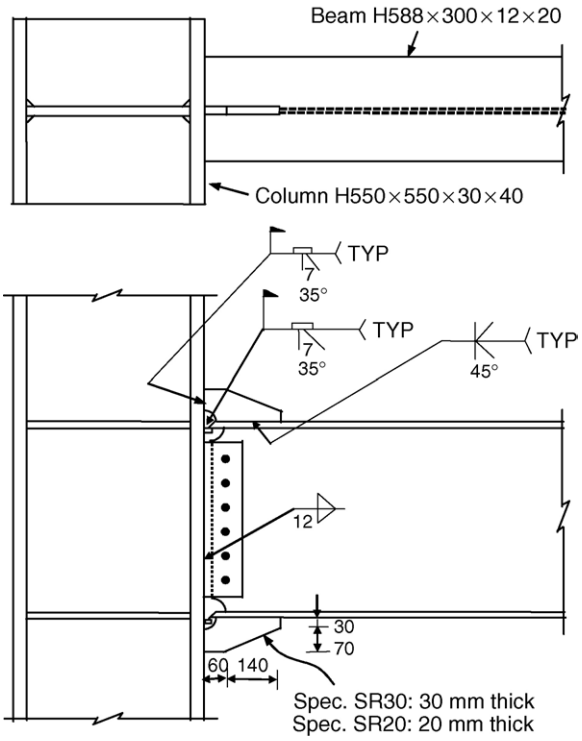

Fig. 18. Connection details for two rib-reinforced specimens.

Fig. 19. Specimen SR30 after failure.

Both specimens failed because of the crack initiated in the beam flange at the rib tip. The formation of this crack was consistent with the results of the finite element analysis,

Fig. 20. Specimen SR20 after failure.

which revealed that the von Mises stress was maximum at the rib tip as observed in the SR connection. The concentration of stress owing to the presence of the rib caused the rib-reinforced connection to fail in the beam flange at the rib tip.

4.2.2. Rotation capacity

Fig. 21 plots moment versus total plastic rotation curves of both rib-reinforced specimens. Notably, the plotted moment was also normalized with respect to the measured plastic moment capacity of the beam. The cyclic behaviour of specimen SR30 was stable, as evidenced by the shape of the hysteresis loops, even though ductile cracks developed in the beam flange at the rib tip. The deterioration in strength indicated by the hysteresis curve was primarily attributable to the local buckling of the beam flanges and the formation of ductile cracks. Specimen SR30 achieved a total plastic rotation of 3.4% rad with a strength that continued to exceed the plastic flexural strength of the beam. Fig. 21(b) shows the moment-rotation response of specimen SR20. The brittle fracture of the beam flange caused specimen SR20 to exhibit an unsatisfactory total plastic rotation of +1.7% and −1.3% rad.

5. Conclusions

The results of finite element analyses and experiments conducted to elucidate the cyclic behaviour of the beam-to-column welded moment connections support the following important conclusions.

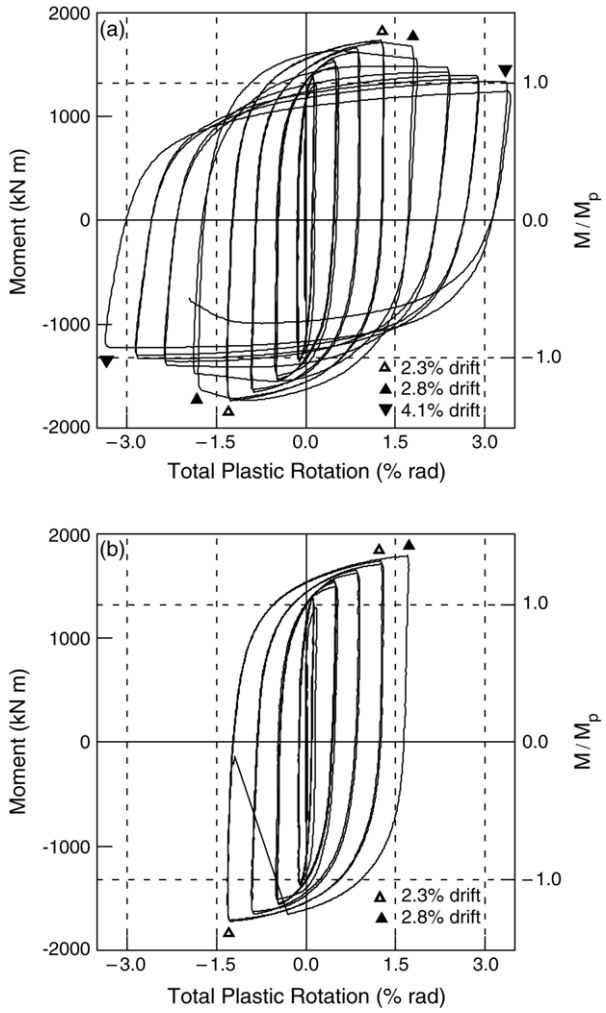

Fig. 21. Hysteresis curves of rib-reinforced connection specimens: (a) specimen SR30; (b) specimen SR20.

1. Tests of two unreinforced specimens revealed moderate inelastic behaviour but failed in a brittle manner under cyclic loading. The fracture of the beam flange near the weld access hole and CJP weld regions caused failure.
2. Finite element analysis of the unreinforced connection showed a localized concentration of stress at the root of the weld access hole, causing the beam flange to fracture.
3. Finite element analysis proved that the rib-reinforced connection can reduce the stress concentration in the access hole region as well as the stress demand in the beam CJP groove weld. Furthermore, a single rib is more effective than double spaced ribs for reducing the localized stress concentration near the weld access hole.

4. Tests of the two specimens rib-reinforced by a single rib welded on each beam flange exhibited the effectiveness of the single rib in preventing beam flange fracture at the root of the weld access hole. One specimen exhibited stable hysteretic behaviour, whereas the other failed by a brittle fracture in the beam flange at the rib tip.

Acknowledgements

The authors would like to thank the Sinotech Engineering Consultants, Inc., for financially supporting this research.

References

[1] Miller DK. Lessons learned from the Northridge earthquake. Engineering Structures 1998;20(4–6):249–60.
[2] Mahin ST. Lessons from damage to steel buildings during the Northridge earthquake. Engineering Structures 1998;20(4–6):261–70.
[3] Tremblay R, Timler P, Bruneau M, Filiatrault A. Performance of steel structures during the 1994 Northridge earthquake. Canadian Journal of Civil Engineering 1995;22:338–60.
[4] Engelhardt MD, Sabol TA. Reinforcing of steel moment connections with cover plates: benefits and limitations. Engineering Structures 1998;20(4–6):510–20.
[5] Uang CM, Yu QS, Noel S, Gross J. Cyclic testing of steel moment connections rehabilitated with RBS or welded haunch. Journal of Structural Engineering, ASCE 2000;126(1):57–68.
[6] Yu QS, Uang CM, Gross J. Seismic rehabilitation design of steel moment connection with welded haunch. Journal of Structural Engineering, ASCE 2000;126(1):69–78.
[7] Kim T, Whittaker AS, Gilani ASJ, Bertero VV, Takhirov SM. Experimental evaluation of plate-reinforced steel moment-resisting connections. Journal of Structural Engineering, ASCE 2002;128(4):483–91.
[8] Plumier A. The dogbone: back to the future. Engineering Journal, AISC 1997;34(2):61–7.
[9] Chen SJ, Yeh CH, Chu JM. Ductile steel beam-to-column connections for seismic resistance. Journal of Structural Engineering, ASCE 1996;122(11):1292–9.
[10] Jones SL, Fry GT, Engelhardt MD. Experimental evaluation of cyclically loaded reduced beam section moment connections. Journal of Structural Engineering, ASCE 2002;128(4):441–51.
[11] Recommended seismic design criteria for new steel moment-frame buildings. Report No. FEMA-350. Federal Emergency Management Agency; 2000.
[12] Guidelines for seismic testing of components of steel structures. Report ATC-24, Applied Technology Council. Redwood City: CA; 1992.
[13] Stojadinovic B, Goel SC, Lee KH, Margarian AG, Choi JH. Parametric tests on unreinforced steel moment connections. Journal of Structural Engineering, ASCE 2000;126(1):40–9.
[14] Azuma K, Kurobane Y, Makino Y. Cyclic testing of beam-to-column connections with weld defects and assessment of safety of numerically modeled connections from brittle fracture. Engineering Structures 2000; 22:1596–608.
[15] ANSYS User Manual. ANSYS, Inc., 2001.
[16] SAC Joint Venture. Interim guidelines: evaluation, repair, modification and design of welded steel moment frame structures. Rep. No. SAC-95-02; 1995.
[17] Engelhardt MD, Sabol TA, Aboutaha RS, Frank KH. Testing connections. Modern Steel Construction, AISC 1995;35(5):36–44.
[18] El-Tawil S, Mikesell T, Kunnath SK. Effect of local details and yield ratio on behavior of FR steel connections. Journal of Structural Engineering, ASCE 2000;126(1):79–87.